

Global Phase Diagrams of Mixed Surfactant–Polymer Systems at Interfaces

Xavier Châtelier^{†,‡,§} and David Andelman^{*,†}

School of Physics and Astronomy, Raymond and Beverly Sackler Faculty of Exact Sciences, Tel Aviv University, Tel Aviv 69978 Israel, and Department of Materials and Interfaces, Weizmann Institute of Science, Rehovot 76100 Israel

Received: December 12, 1995[⊗]

Insoluble surfactant monolayers at the air/water interface undergo a phase transition from a high-temperature homogeneous state to a low-temperature demixed state, where dilute and dense phases coexist. Alternatively, the transition from a dilute phase to a dense one may be induced by compressing the monolayer at constant temperature. We consider the case where the insoluble surfactant monolayer interacts with a semidilute polymer solution solubilized in the water subphase. The phase diagrams of the mixed surfactant/polymer system are investigated within the framework of mean field theory. The polymer enhances the fluctuations of the monolayer and induces an upward shift of the critical temperature. The critical concentration is increased if the monomers are more attracted (or at least less repelled) by the surfactant molecules than by the bare water/air interface. In the case where the monomers are repelled by the bare interface but attracted by the surfactant molecules (or vice versa), the phase diagram may have a triple point. The location of the polymer special transition line appears to have a big effect on the phase diagram of the surfactant monolayer.

1. Introduction

Understanding the subtle interactions between macromolecules, such as polymer or proteins, and amphiphiles, such as surfactants or phospholipids, has been a problem of prime interest in recent years in many industrial applications and in biological systems. For instance, biomembranes^{1,2} are usually depicted as fluid bilayers composed of different constituents: phospholipids, cholesterol, and proteins. In addition, a complex macromolecular network (*the cytoskeleton*) is associated with the inner side of the bilayer and modifies the mechanical properties of the membrane, while the glycocalix, on the outer side, is believed to play an important role in molecular recognition. In industry, surfactants are used in a wide range of applications (detergents, soaps, oil recovery, paints) where polymers are often added in order to provide stability for the system, especially in the case of colloidal suspensions and oil/water emulsions.³ Those mixed polymer and surfactant systems tend to create complex self-assembly structures (connected micelles, gels, networks, etc.).^{4–6} Finally, drug delivery via microencapsulation is another example where the stability of surfactant vesicles is improved by the adsorption of polymer.⁷

In recent years, a new category of *associating* polymers has been introduced. Those are the hydrophobically modified water-soluble polymers (HM-WSP), consisting of a water soluble polymer backbone carrying small hydrophobic side chains. Such polymers present interesting properties of self-association, which may even be enhanced by the addition of surfactant, and are very useful as viscosity modifiers of aqueous solutions.⁸ The subtle coupling between the surfactant and the polymer may lead to unusual phenomena like thermogelation,⁹ where gelation of the system is obtained upon increasing of the temperature. Such systems have been studied theoretically¹⁰ as well as experimentally in the bulk. However, little is known about their behavior at interfaces.¹¹

In the present work, the interaction of water-soluble polymers with a surfactant monolayer located at the air/water interface is considered. We restrict ourselves to the relatively simple situation of an insoluble surfactant monomolecular layer (*Langmuir monolayer*). Langmuir monolayers have been used in many applications,^{12,13} from evaporation control to nonlinear optic devices (via the creation of *Langmuir–Blodgett monolayers*). They are also used to study crystallization of solids¹⁴ and provide useful model systems for more complicated fluctuating liquid interfaces (membranes) where curvature effects cannot be neglected.

Another motivation for the present study comes from the lack of understanding of adsorption (or depletion) of polymers close to nonideal interfaces, as compared with adsorption on ideal (namely, perfectly flat and chemically homogeneous) surfaces. On ideal surfaces^{15–19} theories for neutral and flexible polymers in good solvent have been performed (both for adsorption and depletion) and compared with scaling theories. For nonideal surfaces, much less theoretical works exists. It has been suggested that the bending properties of a curved interface are modified in the presence of adsorbing polymer.^{20–22} When the polymer adsorbs on both sides of the interface (a bilayer, for instance), the curvature modulus decreases, while the saddle-splay modulus increases. When it adsorbs only on one side, a nonzero spontaneous curvature is induced. The situation of a perfectly flat but chemically heterogeneous interface has been considered only in a few works.^{22–25} The case of annealed disorder (namely, when the disorder is at thermodynamic equilibrium and the heterogeneities can diffuse laterally) is found to behave differently from the case of quenched disorder (where heterogeneities are spatially “frozen”). However, in both cases the adsorption of the polymer is increased by the nonideality of the surface. In this context, a surfactant monolayer is an example of a nonideal annealed surface, where the order parameter is the local surfactant surface concentration.

The phase diagram of surfactant monolayers can be constructed as a function of the thermodynamical variables:¹² surface pressure and temperature (or equivalently area per molecule and temperature). At low surface pressure, a phase separation occurs (for temperatures below the corresponding

[†] Tel Aviv University.

[‡] Weizmann Institute of Science.

[§] Present address: CRM-ICS, 6, rue Boussingault, 67083 Strasbourg Cedex, France.

[⊗] Abstract published in *Advance ACS Abstracts*, March 15, 1996.

critical temperature). Dilute (gaseous) and dense (liquid-expanded) regions of the monolayer coexist, in analogy to phase transitions in the bulk. In the phase diagram, single-phase and two-phase regions are separated by a coexistence curve. At higher surface pressure, other phase transitions occur. Depending on the symmetries of the specific surfactant molecules, the phase diagrams are more complex and still a topic of current investigation.^{26,27}

In the following, we consider how a simple condensation transition (gas to liquid expanded) of a surfactant monolayer at the air/water interface is affected by the presence of polymer in the water subphase. The free energy and the assumptions used in deriving it are introduced in section 2, while in section 3 we discuss the main results, as applied to a simple case; the general theory is detailed in Appendices A and B. Finally, some analytical considerations on the critical point are presented in Appendix C.

2. The Polymer/Surfactant Free Energy

The model used for the mixed surfactant/polymer system follows closely the lattice model introduced in ref 24. The local (dimensionless) free energy per site F , rescaled in units of $k_B T$, where k_B is the Boltzmann constant and T is the temperature, can be separated into three parts: the surfactant contribution F_s , the polymer contribution F_p , and the coupling term F_{ps} :

$$F = F_s + F_p + F_{ps} \quad (2.1)$$

In the following, those three terms are discussed separately.

2.1. The Surfactant Contribution F_s . The monolayer free energy is calculated using a lattice-gas model. Each lattice site is occupied either by a surfactant molecule or by an artificial vacancy, in order to allow us to consider a compressible monolayer. The free energy of a surfactant monolayer is the sum of the enthalpy and entropy of mixing and depends on the monolayer area fraction (or equivalently coverage) c ranging from 0 to 1, $c = A_0/A$, where A_0 is the close-packing area of a surfactant molecule (or the area of one site on the lattice) and A is the actual area per surfactant molecule on the interface. Typically $A_0 \approx 25\text{--}35 \text{ \AA}^2$ for a surfactant molecule.²⁸ Disregarding linear terms, the surfactant free energy F_s (per site and per $k_B T$), within a Bragg–Williams (mean field) theory, is written as

$$F_s = \nu^{-1}c(1-c) + c \log c + (1-c) \log(1-c) \quad (2.2)$$

where ν^{-1} is the dimensionless interaction parameter of the surfactant on the surface and describes van der Waals interactions between neighboring particles. The interactions between the head groups of the surfactant molecules, playing an important role in the determination of the highly compressed phases, as well as the degrees of freedom of conformation for the hydrophobic chains, whose coupling with the surfactant coverage c is determinant in the liquid expanded versus liquid condensed transition,²⁸ are not taken into account. As only short-ranged interactions are considered (between neighboring sites), the surfactant molecules are supposed to be neutral. The main interactions modeled by the parameter ν are the van der Waals interactions.

For an insoluble monolayer, the total number of surfactant molecules is fixed. At low (and positive) values of ν (corresponding to low temperatures), a phase separation between dense and dilute regions follows from eq 2.2. The stability of such a monolayer is obtained by studying the convexity of the free energy.²⁹ The monolayer becomes unstable if the second derivative of the free energy becomes negative. The condition

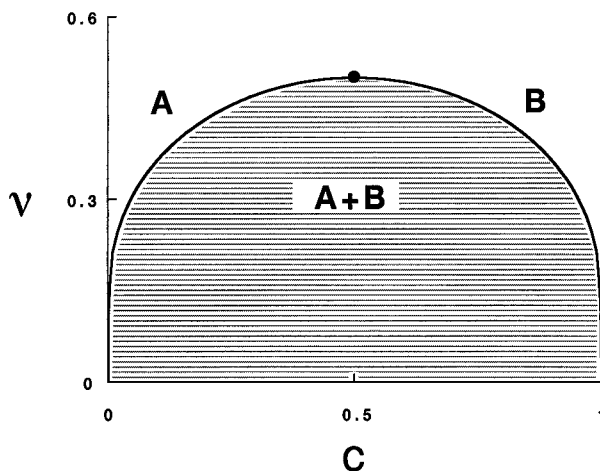


Figure 1. Phase diagram for a bare surfactant monolayer, without polymer in the water subphase. At low ν (low temperatures), the homogeneous state is unstable and the binodal line delimits the two-phase coexistence region labeled A+B. The critical point is located at $\nu_c = 0.5$, $c_c = 0.5$ and is shown by a dot.

$F_s''(c) = 0$ defines the *spinodal line*, separating metastable and unstable regions. The spinodal line obtained from eq 2.2 is $\nu_s^0(c) = 2c(1-c)$, and it lies within the coexistence region of the phase diagram. In addition, the coexisting curve limiting the two-phase region (*the binodal line*) is easily found from eq 2.2 as the system is symmetric about $c = 0.5$:

$$\nu_b^0(c) = -\frac{1-2c}{\log c - \log(1-c)} \quad (2.3)$$

The spinodal and binodal lines join together at the critical point $c = 0.5$, $\nu_c = 0.5$. In Figure 1 the binodal line and the critical point are shown for a pure surfactant monolayer.

2.2. The Polymer Contribution F_p . The polymer in the subphase is assumed to be neutral and flexible as well as in good solvent conditions, hence has a positive second virial coefficient and no polymer–solvent phase separation. For a semidilute polymer solution, a mean field theory applied to the Edwards density functional method is commonly used.^{19,30} The free energy density is conveniently expressed as a function of the variable $\phi(z)$ related to $c_p(z)$, the local monomer concentration, by $\phi^2(z) = c_p(z)/c_b$. The coordinate z denotes the perpendicular distance from the interface, and $c_b = c_p(z \rightarrow \infty)$ is the concentration of the polymer in the bulk (acting as a reservoir). The characteristic length in the solution is the Edwards correlation length $\xi = a/\sqrt{3\nu c_b}$, where ν is the excluded volume parameter (positive, in good solvent conditions), and the typical energy parameter (per $k_B T$) for the interactions between monomers in the bulk is $\epsilon_p = A_0 \xi \nu c_b^2$. Using these notations, the free energy per site reads

$$F_p = \frac{\epsilon_p}{2} \int_0^\infty dz \left(\xi (\nabla \phi)^2 + \frac{1}{\xi} (\phi^2 - 1)^2 \right) \quad (2.4)$$

The first term accounts for the elastic flexibility of the polymer chains, and the second originates from the excluded volume interaction combined with the equilibrium condition with the polymer bulk reservoir. The polymer free energy F_p is a functional of the polymer profile $\phi(z)$ and of the order parameter at the interface $\phi_s = \phi(z=0)$. It does not include the energy of interaction with the surface, discussed separately below.

Minimizing F_p with respect to the polymer profile $\phi(z)$, leaving the surface value as a free parameter, yields the polymer profile $\phi(z) = \coth(z/\xi + b)$, where b is a constant of integration

related to ϕ_s by $\phi_s = \coth b$, in the case of adsorption ($\phi(z) > 1$), and $\phi(z) = \tanh(z/\xi + b')$ in the case of depletion ($\phi(z) < 1$), where, similarly, $\phi_s = \tanh b'$. For both adsorption and depletion, the free energy F_p for the optimal profile is

$$F_p = \frac{\epsilon_p}{3}(\phi_s^3 - 3\phi_s + 2) = \frac{\epsilon_p}{3}(\phi_s - 1)^2(\phi_s + 2) \quad (2.5)$$

and has a minimum at $\phi_s = 1$. This means that the polymer solution would like to be homogeneous throughout the solution at the imposed bulk value $c_p(z) = c_b$. The only possibility of obtaining a profile with $\phi_s \neq 1$ is due to the short range coupling of the polymer with the surface. This coupling includes the surfactant monolayer as well as the bare air/water interface. It is given below by the term F_{ps} .

A quantity accessible to experiment which measures the total adsorption of the monomers at the interface is the polymer surface excess defined as $\Gamma = \int_0^\infty dz (c_p(z) - c_b)$. Using the above results of the minimization for the polymer profile (mean-field theory), it is simply related to ϕ_s by

$$\Gamma = c_b \xi (\phi_s - 1) \quad (2.6)$$

Note that if ρ is the volume fraction of the monomers in the bulk solution, a naive calculation starting from $c_b \approx \rho/a^3$ (where a is the size of a monomer) yields $\epsilon_p \approx \rho^{3/2}$. For a semidilute polymer solution, $N^{-4/5} \ll \rho \ll 1$ (where N is the number of monomers in a chain). Hence, roughly, for $N = 10^4$ the range for typical values of ϵ_p is given³¹ by $10^{-4} < \epsilon_p < 10^{-1}$.

Although the self-consistent field theory provides a convenient and qualitatively correct framework for the description of the semidilute polymer solution, some of its predictions (like the form of the polymer profile $c_p(z)$ for instance) are in disagreement with a scaling theory.¹⁹ Nevertheless, we will use it to model the polymer behavior in solution.

2.3. The Coupling Term F_{ps} . A bilinear term in the surfactant and monomer concentrations at the interface ($z = 0$) is a simple, yet meaningful, phenomenological coupling for the polymer–interface interaction, which is assumed to be short-ranged:

$$F_{ps} = -\frac{1}{2}[\alpha_0 c + \gamma_0(1 - c)]\phi_s^2 = -\frac{1}{2}\epsilon_{ps}(c - c^*)\phi_s^2 \quad (2.7)$$

α_0 is the polymer/surfactant interaction parameter, and γ_0 is the polymer/bare interface interaction parameter. In eq 2.7, we define the “effective” polymer/surfactant interaction parameter $\epsilon_{ps} \equiv \alpha_0 - \gamma_0$. It is positive whenever the monomers interact more favorably with the surfactant molecules than with the bare water/air interface. The *special transition* coverage is defined as $c^* \equiv \gamma_0/(\alpha_0 - \gamma_0)$ as long as $\gamma_0 \pm \alpha_0$. In principle, those parameters can depend on temperature.

The phenomenological coupling F_{ps} can be justified for polymers in the semidilute regime since in such systems the monomer concentration is small with respect to unity. However, it represents only the lowest term in an expansion in the surfactant concentration at the interface. When $\epsilon_{ps} > 0$, the F_{ps} term corresponds to a repulsion of the polymer from the surface (depletion) for $c < c^*$ and to an attraction to the surface (adsorption) for $c > c^*$. The special transition line $c = c^*$ occurs for physical values of the coverage, $0 < c^* < 1$, when the attraction (repulsion) of the monomers with the surfactant molecules is in competition with the repulsion (attraction) with the bare interface. In the $0 < c^* < 1$ range, a positive α_0 is equivalent to having a positive ϵ_{ps} and means that the interaction between the monomers and the surfactant molecules is attractive.

2.4. The Total Free Energy F . Combining all three contributions, $F_s + F_p + F_{ps}$, we obtain the total free energy (per site of the interface and per $k_B T$):

$$F = \nu^{-1}c(1 - c) + c \log c + (1 - c) \log(1 - c) + \frac{1}{3}\epsilon_p(\phi_s - 1)^2(\phi_s + 2) - \frac{1}{2}\epsilon_{ps}(c - c^*)\phi_s^2 \quad (2.8)$$

Note that the energy is invariant under the transformation $\epsilon_{ps} \rightarrow -\epsilon_{ps}$, $c \rightarrow 1 - c$ and $c^* \rightarrow 1 - c^*$. Therefore, it will be assumed in the following that $\epsilon_{ps} > 0$ without loss of generality.

The free energy F is a function of ϕ_s and c . Minimizing it first with respect to the polymer surface order parameter ϕ_s (mean field approximation), we obtain

$$\phi_s = \frac{\lambda}{2\epsilon_p} + \sqrt{\left(\frac{\lambda}{2\epsilon_p}\right)^2 + 1} \quad (2.9)$$

where $\lambda = \epsilon_{ps}(c - c^*) = \alpha_0 c + \gamma_0(1 - c)$ measures the strength of the interaction between the polymer and the overall interface (including the bare interface as well as the surfactant). Equation 2.9 relates $\phi_s^2(c)$, the concentration of monomers at the interface, with the surfactant area fraction c . Consequently, the entire polymer profile and the polymer surface excess can be found as a function of the surfactant concentration on the interface.

The limit of a very strong adsorption, $\lambda/\epsilon_p \rightarrow \infty$ (e.g., $c^* \ll 0$), yields $\phi_s \approx \lambda/\epsilon_p \gg 1$. On the other hand, the limit of very strong depletion, $\lambda/\epsilon_p \rightarrow -\infty$ (e.g., $c^* \gg 1$), yields $\phi_s \approx |\epsilon_p/\lambda| \ll 1$. For $\lambda/\epsilon_p \rightarrow 0$ (e.g., $c \rightarrow c^*$), $\phi_s \rightarrow 1$, which means that the polymer solution remains homogeneous: $c_p(z) = c_b$, even at the surface. As is shown in Figure 2a, the special transition line $c = c^*$ divides the parameter range into an adsorption region ($c > c^*$) and a depletion one ($c < c^*$).

If the surfactant monolayer is in the two-phase region, dilute and condensed regions of the surfactant coexist and the polymer adsorbs differently on those regions because of its different affinity as described by the parameter $\epsilon_{ps} > 0$. Note that since the curve $\phi_s(c)$ is convex (see Figure 2b), the polymer surface excess is enhanced when the surfactant monolayer undergoes a phase separation. Qualitatively, the convexity of the curve $\phi_s(c)$ indicates²⁴ that the surfactant concentration fluctuations increase the average polymer surface concentration ϕ_s and, hence, the polymer surface excess $\Gamma \sim \phi_s - 1$.

Equation 2.9 shows how the surfactant molecules affect the polymer adsorption. The main remaining task is to understand how the polymer itself affects the phase diagram of the surfactant monolayer, since the two problems are coupled. Using eq 2.9, $\phi_s = \phi_s(c)$, the total free energy can be written only as a function of the surfactant coverage c :

$$F(c) = F_s(c) - \frac{\epsilon_p}{6}(\phi_s^2 + 3)\phi_s \quad (2.10)$$

The study of the convexity of the total free energy $F(c)$ as a function of c (the only remaining order parameter) determines the location of the *modified* spinodal line. Similarly, the full phase diagram can be obtained numerically from a common-tangent construction of $F(c)$.

For the sake of clarity, the main physical features can be illustrated in a simple situation. This is done in the next section, where ϵ_p , c^* , and $\nu\epsilon_{ps}$ are taken to be independent of the temperature T and $\nu \sim T$. A more general treatment without any assumptions on the T -dependence of the interaction parameters is presented in Appendices A and B.

3. Results

3.1. T -Dependence of the Interaction Parameters. T/ν is independent of the temperature if we assume that the interaction

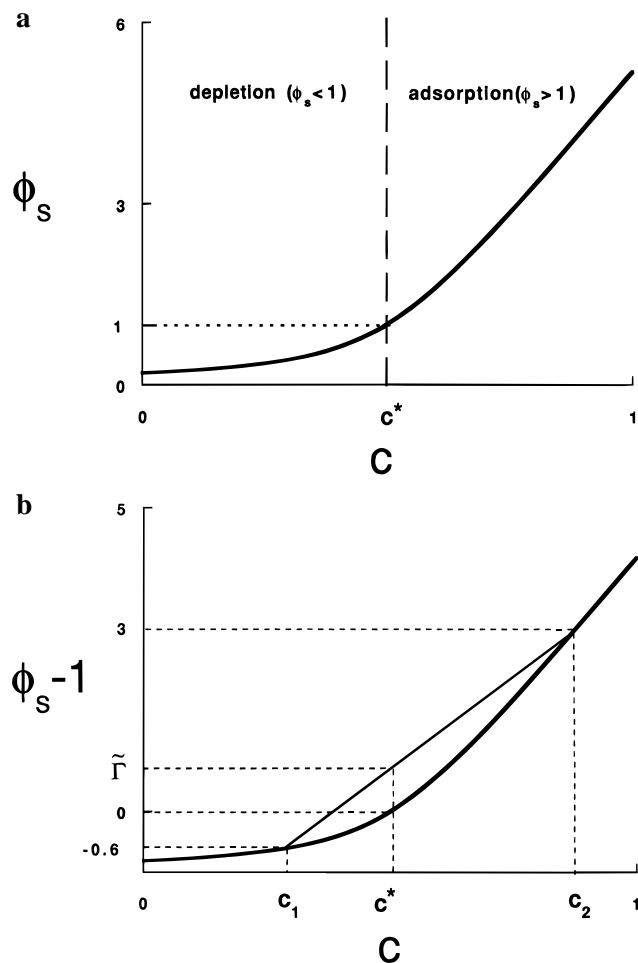


Figure 2. (a) Polymer order parameter ϕ_s and (b) polymer surface excess, $\tilde{\Gamma} \equiv \Gamma/(c_b \xi) = \phi_s - 1$, as a function of the surfactant coverage c for $\epsilon_{ps}/\epsilon_p = 10$ and $c^* = 0.5$. In (a) the special transition line divides the region where the polymer is adsorbed ($c > c^*$) from the region where it is depleted ($c < c^*$). In (b), for homogeneous monolayers of concentrations $c_1 = 0.29$, $c_2 = 0.875$, and $c^* = 0.5$, the polymer surface excess is respectively -0.6 , 3 , and 0 . Due to the convexity of the curve, for a surfactant monolayer of average concentration c^* demixing between coexisting regions of concentration c_1 and c_2 , the surface excess $\tilde{\Gamma}$ is positive.

potential of the surfactant molecules has an infinite repulsive core followed by a weak attraction independent of the temperature, $0 < w \ll k_B T$. In such a case, the surfactant second virial coefficient is given by $\nu_s = 1 - w/(k_B T)$. Expanding the energy F_s , eq 2.2, in powers of c shows that the virial expansion²⁹ is equivalent to the Bragg–Williams theory (at low concentrations) with $\nu^{-1} = w/(k_B T)$. Thus $k_B T/\nu$ is independent of the temperature. Note that the strength of this attraction w is related to the critical temperature of the pure surfactant monolayer by $w = \nu_c^{-1} k_B T_c = 2k_B T_c$.

For the semidilute polymer solution, taking only excluded volume interactions between monomers and assuming an athermal solvent, ν and ϵ_p are independent of T .

We also assume that the interaction between the monomers and the bare interface is independent of the temperature, resulting in $\gamma_0 \sim 1/T$ since the dimensionless γ_0 is rescaled in units of $k_B T$. In a similar manner, neglecting the steric effects between the monomers and the surfactant molecules, and assuming that the monomer/surfactant interactions are attractive, weak, and short-ranged, results in $\alpha_0 \sim 1/T$. Under these conditions $\nu\epsilon_{ps}$ and c^* are independent of T .

In conclusion, the phase diagram in the simplified case can be plotted in the (ν, c) plane and is a cut of the *global* phase

diagram (presented in the appendices) plotted in the $(\nu, c, \epsilon_p, \nu\epsilon_{ps}, c^*)$ space. The next subsections will present some features of this simplified case.

3.2. The (ν, c) Phase Diagram. We limit ourselves to $\nu > 0$, $\epsilon_p > 0$ and $\epsilon_{ps} > 0$; $\nu > 0$ corresponds to an attraction between the surfactant molecules; $\epsilon_p > 0$ follows from the assumption that the polymer is in a good solvent (its excluded volume parameter ν is positive), and $\epsilon_{ps} > 0$ can be used without loss of generality, as was explained in section 2.4. The spinodal line $\nu_s(c)$ of the mixed surfactant–polymer system is obtained from the condition

$$\frac{\partial^2 F}{\partial c^2} = -2\nu^{-1} + \frac{1}{c(1-c)} - \frac{\epsilon_{ps}^2}{\epsilon_p} \frac{\phi_s^3(c)}{\phi_s^2(c) + 1} = 0 \quad (3.1)$$

The critical point is the extremum point on the spinodal, satisfying in addition

$$\frac{\partial^3 F}{\partial c^3} = 0 \quad (3.2)$$

Equation 3.1 shows that the spinodal temperature ν_s is shifted upward²⁴ and the region of instability is increased. Physically, this general effect comes from the indirect attractive interaction between the surfactant molecules induced by the polymer, and was already explained elsewhere.²² Here, it is represented by the term $-\epsilon_p(\phi_s^3 + 3\phi_s)/6$ in the free energy. It is bigger for larger values of the surfactant concentration c because $\phi_s(c)$ is an increasing function of c . Consequently, the phase diagram is no longer symmetric around $c = 1/2$. The shift on the spinodal and binodal lines is bigger for the large values of c and the critical point is shifted to a concentration $c_c > 1/2$.

In the following, we discuss several limits and try to show that (except in the low-coupling limit) the position of the special transition line $c = c^*$ in the (ν, c) plane crucially affects the phase diagram. This can be checked easily in the limits of very high and very low surfactant concentration, where the scaling of the spinodal temperature ν_s is analytically derived and depends on the relative position of the spinodal line with respect to the special transition line.

3.3. The Limits $c \rightarrow 0$ and $c \rightarrow 1$. Three cases can be distinguished in the $c \rightarrow 0$ limit of the spinodal line:

1. If $c^* > 0$, the polymer is strongly depleted from the interface. The shift of the spinodal temperature $\nu_s(c)$ from the pure value $\nu_s^0(c)$ is small and scales as $\nu_s - \nu_s^0 \sim c^3$, where $\nu_s^0 = 2c(1-c)$ is the pure surfactant spinodal line (no added polymer).

2. On the other hand, if $c^* < 0$, the polymer is strongly attracted by the interface and ν_s scales as $\nu_s \sim c^{1/3}$.

3. In the special case when $c^* = 0$, the polymer solution remains homogeneous. The dominant term in the spinodal equation also changes and ν_s scales as $\nu_s \sim c^{1/2}$.

The scaling of the spinodal temperature in the limit $c \rightarrow 1$ depends similarly on the position of the special transition line relatively to the line $c = 1$. In the following, the other regions of the phase diagram are considered and ν is at least of order unity.

3.4. The Low-Coupling Limit: $\nu\epsilon_{ps} \ll 1$. In the case when $\nu\epsilon_{ps}$ is small enough,³² the third term in spinodal equation 3.1 is negligible. The phase diagram is very similar to that of the pure surfactant monolayer (see Figure 1). The spinodal temperature $\nu_s(c)$ as well as the binodal temperature $\nu_b(c)$ can be

expanded in powers of $\nu\epsilon_{ps}$. To second order in $\nu\epsilon_{ps}$, the shift of the binodal line is identical to the shift of the spinodal line:

$$\nu_s(c) - \nu_s^0(c) = \nu_b(c) - \nu_b^0(c) = \frac{1}{4\epsilon_p}(\nu\epsilon_{ps})^2 \quad (3.3)$$

For the low-coupling limit, the critical temperature is shifted upward²⁴ by a factor of order $(\nu\epsilon_{ps})^2$. Note that, to second order in $\nu\epsilon_{ps}$, the shift is independent of the surfactant area fraction and the special transition coverage c^* . The critical concentration c_c is also shifted upward, but only to third order in $\nu\epsilon_{ps}$:

$$c_c - 1/2 = \frac{1}{8\epsilon_p^2}(\nu\epsilon_{ps})^3 \quad (3.4)$$

Another case where the third term in spinodal equation 3.1 is negligible is when $\phi_s(c) \ll 1$. Here, the polymer is very strongly depleted from the interface. This occurs, for instance, when $\epsilon_p \ll 1$ and $c < c^*$.

3.5. The Strong-Coupling Limit: Large Values of $\nu\epsilon_{ps}$. We define the strong-coupling limit as the situation when the spinodal line is strongly shifted upward, $\nu_s(c) \gg 1$ and the first term in spinodal equation 3.1 is negligible. ϵ_{ps} is the only parameter left in the equation depending on the temperature. As $\nu = (\nu\epsilon_{ps})/\epsilon_{ps}$, the temperature on the spinodal line is proportional to the parameter $\nu\epsilon_{ps}$ and the coefficient of proportionality ϵ_{ps}^{-1} is obtained from spinodal equation 3.1 rewritten as a fifth order equation for ϵ_{ps} depending on ϵ_p , c^* , and c (and independent of $\nu\epsilon_{ps}$):

$$4\left(\frac{\epsilon_p}{c(1-c)}\right)^2 + \left(\frac{c-c^*}{c(1-c)}\right)^2 \epsilon_{ps}^2 - 4\frac{c-c^*}{c(1-c)}\epsilon_{ps}^3 - \epsilon_{ps}^4 - \frac{(c-c^*)^3}{\epsilon_p^2 c(1-c)}\epsilon_{ps}^5 = 0 \quad (3.5)$$

Whenever eq 3.5 has a unique positive solution ϵ_{ps} , the approximation of the strong coupling limit is self-consistent provided that $\nu\epsilon_{ps} \gg \epsilon_{ps}$. This is the case for $c \geq c^*$. On the other hand, when the polymer is depleted from the interface (corresponding to $c < c^*$), there is a minimal value of c for which eq 3.5 has a positive solution. Indeed, a sufficient condition for eq 3.5 not to have any positive solution is:

$$c^* - c > \left(\frac{11}{1350 + 210\sqrt{42}}\right)^{1/4} \sqrt{\epsilon_p} \approx 0.2524\sqrt{\epsilon_p} \quad (3.6)$$

This implies that, in a system where condition 3.6 is respected for the largest physical c value, $c = 1$, the strong-coupling limit cannot be defined and the critical temperature ν_c is necessarily of order unity.

When $c^* \rightarrow -\infty$ or when $\epsilon_p \rightarrow 0$ (and $c > c^*$), the solution of eq 3.5 is small, $\epsilon_{ps} \ll 1$. In this situation, $\nu\epsilon_{ps}$ of order unity is enough to ensure that $\nu_s \gg 1$ and

$$\nu_s(c) = \nu\epsilon_{ps}(c - c^*)^{1/3}[c(1 - c)]^{1/3}\epsilon_p^{-2/3} \quad (3.7)$$

In the strong-coupling limit, the binodal line is also proportional to the coupling parameter $\nu\epsilon_{ps}$. Numerical solution of eqs 3.1 and 3.2 indicates that the behavior of the binodal line is simpler than the one of the spinodal line. In particular, if the strong coupling limit can be defined only over a range of surfactant coverage c (for instance, when the special transition line intersects the phase diagram), then the binodal line is found to be proportional to $\nu\epsilon_{ps}$ for all values of c (except for the limiting values $c \rightarrow 0$ or for $c \rightarrow 1$). Figure 3 shows the

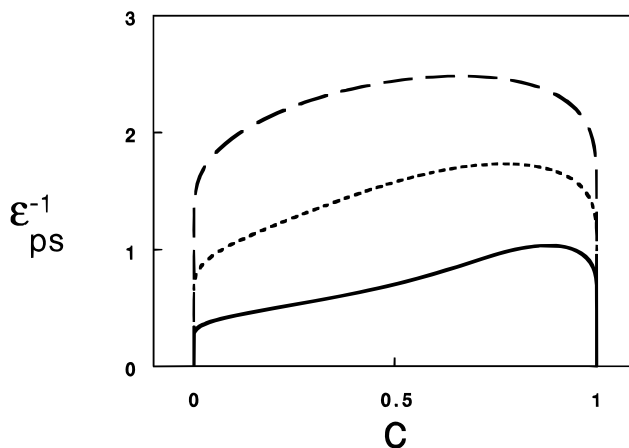


Figure 3. Value of ϵ_{ps}^{-1} on the binodal line in the strong-coupling limit (independent on ν) for $c^* = 0$ (dashed line), $c^* = 0.5$ (dotted line), and $c^* = 0.8$ (full line) at a fixed value of the polymer interaction parameter $\epsilon_p = 0.1$. The binodal temperature ν is directly related to ϵ_{ps}^{-1} by $\nu = (\nu\epsilon_{ps})\epsilon_{ps}^{-1}$. When c^* decreases, the polymer interacts more favorably with the interface and its effect on the phase diagram of the surfactant monolayer is stronger: the binodal temperature increases.

dependence of the binodal temperature on the special transition value c^* , at a fixed value of the polymer interaction parameter ϵ_p . Lower values of the special transition coverage c^* correspond, for a fixed coupling $\nu\epsilon_{ps}$, to a higher binodal temperature.

3.6. High Polymer Flexibility, $\epsilon_p \ll 1$; Possibility of a Triple Point. As was explained in section 2, ϵ_p is likely to be very small for a semidilute polymer solution. When $\epsilon_p \ll 1$, the strong-coupling limit is obtained for $c > c^*$ (as was explained in section 3.5) and the polymer is strongly adsorbed at the interface (see Figure 3). On the other hand, for $c < c^*$, the polymer is depleted from the interface and the situation is a one of low coupling. Consequently, the features of the phase diagram are particularly sensitive to the position of the special transition line: when $c^* > 1$, the phase diagram is very close to the one of the pure surfactant monolayer (see Figure 1), while for $c^* < 0$ the spinodal line is given by eq 3.7 and the binodal temperature is strongly shifted upward. When the special transition line intersects the phase diagram, there is a competition between the two types of phase behavior. In section 3.5, it was mentioned that the phase diagram of the strong coupling is dominant in that situation.

More precisely, an expansion of the free energy in powers of ϵ_p/ϵ_{ps} shows that, for $c > c^*$, $F(c) \approx -1/6(\epsilon_{ps}^3/\epsilon_p^2)(c - c^*)^3$, while for $c < c^*$, it yields $F(c) \approx F_s(c)$. Figure 4a shows a plot of the free energy in a case where this sudden decrease of $F(c)$ for $c > c^*$ is particularly well defined. When $c^* > 1/2$, the binodal line of the pure surfactant monolayer can be obtained with a common tangent construction (in the range of temperatures where the two coexistence concentrations are lower than the special transition coverage c^*). However, it corresponds to a metastable state. There is yet a second pair of coexisting concentrations which leads to an even lower free energy.

When $0 < c^* < 1$, the phase diagram of the strong-coupling limit predominates over the one of the pure surfactant monolayer, while for $c^* > 1$ this is not the case anymore. For physical values of the parameters, the transition between the two regimes, occurring around $c^* = 1$, is smooth. In some situations, the two pairs of coexisting concentrations mentioned above are stable and correspond to two first-order phase transitions, as is shown in Figure 4b. The total phase diagram exhibits two critical points and one triple point. An example of such a phase diagram with a triple point is presented in Figure

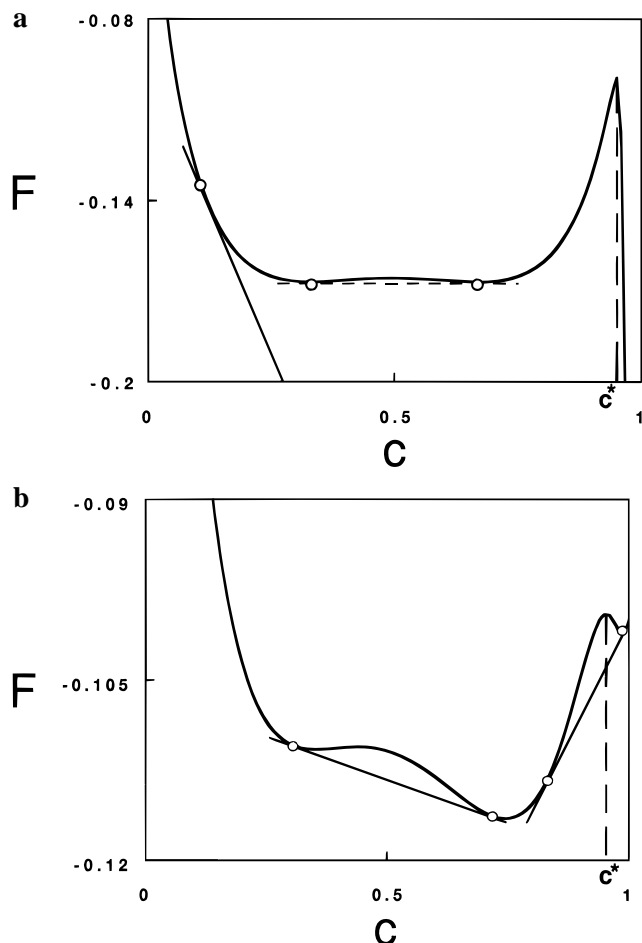


Figure 4. Free energy F as a function of the surfactant concentration c at the interface for $\nu = 0.48$, $\nu\epsilon_{ps} = 1$, $c^* = 0.95$. In (a) $\epsilon_p = 0.02$ and in (b) $\epsilon_p = 0.1$. The common tangent construction is shown by thin lines, and the coexistence values are shown by circles. In (a), in the region $0 < c < c^*$, the plot is similar to the case of the pure surfactant monolayer. The corresponding coexistence region, $0.33 \leq c \leq 0.67$, is only metastable, since it is contained in the second coexistence region $0.11 \leq c \leq 1.0$. In (b), both coexistence regions $0.31 \leq c \leq 0.72$ and $0.83 \leq c \leq 0.99$ occur.

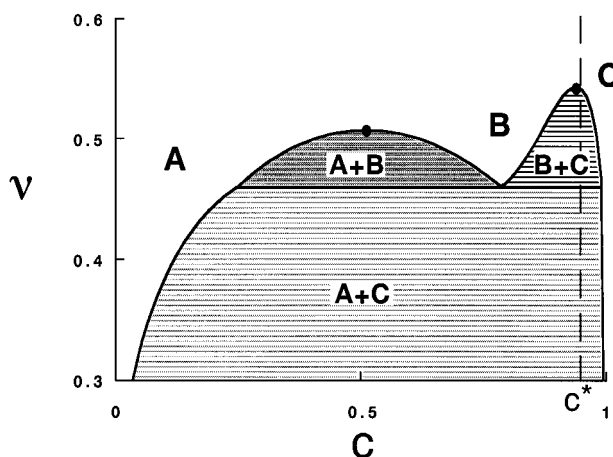


Figure 5. Phase diagram of the surfactant monolayer for $c^* = 0.95$, $\epsilon_p = 0.1$, and $\nu\epsilon_{ps} = 1$. The two-phase region labeled A+B ends at the critical point: $\nu_c = 0.51$, $c_c = 0.50$. The second B+C critical point is located at $\nu_c = 0.53$, $c_c = 0.94$. All three two-phase regions, A+B, A+C, and B+C, join at a triple point— $\nu = 0.46$, $c_A = 0.25$, $c_B = 0.79$, and $c_C = 0.99$ —where all three phases (A, B, and C) coexist. Critical points are shown by a dot.

5. In Figure 6 we show for the same set of parameters three typical isotherms plotted in the reduced surface pressure Π —

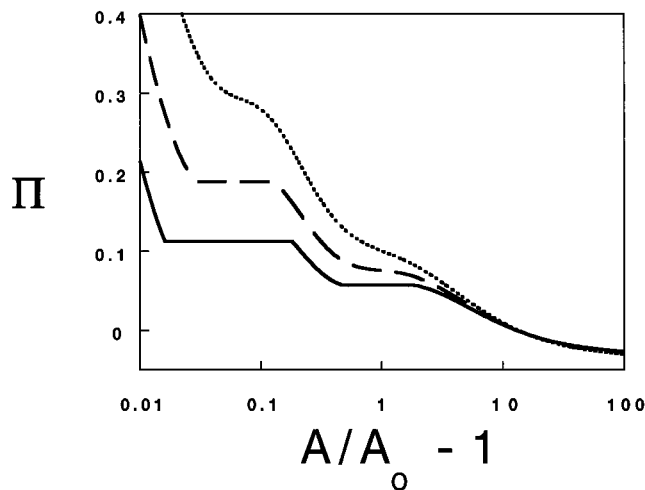


Figure 6. Isotherms for the surfactant monolayer. The reduced surface pressure $\Pi = \nu c^2 \partial(F/c)/\partial c$ is plotted versus the reduced area per molecules $1/c - 1 = A/A_0 - 1$ on a logarithmic scale. A_0 is the close-packing area and F is the total free energy as defined in the text. Three typical isotherms are shown for three different temperatures: $\nu = 0.56$ (dotted line, no phase transition); $\nu = 0.52$ (dashed line, one phase transition); $\nu = 0.49$ (full line, two phase transitions). The other parameters are identical to the ones of Figure 5.

reduced area per surfactant plane. The reduced surface pressure is defined by rescaling the actual surface pressure (*i.e.*, the difference between the bare water/air surface tension and that of the surfactant monolayer) by $A_0\nu/k_B T$, resulting in the relation $\Pi = \nu c^2 \partial(F/c)/\partial c$. Depending on the temperature, the isotherms can have zero, one, or two plateaus corresponding respectively to zero, one, or two coexisting regions.

4. Discussion

In order to derive our model, we assumed several simplifying assumptions. The expression for the surfactant free energy F_s does not take into account the surfactant hydrophobic tail degrees of freedom. The coupling between the tail conformations and the concentration of the surfactant molecules becomes crucial at high surfactant densities and can lead to a rich phase behavior,^{26,27} which was not addressed here. We consider here only the dilute phases of surfactant monolayers: the gaseous phase at low densities and temperatures, the liquid-expanded phase at higher densities, and the condensation transition between them.²⁸

Another limitation of the model comes from our mean-field treatment of the polymer free energy F_p . The assumption that the polymer solution is semidilute may break down close to the interface if the polymer strongly adsorbs. Our approach assumes that $c_p(z=0) \ll 1$ or equivalently $\lambda \ll \rho$, where ρ is the volume fraction of the monomers in the bulk and $\lambda = \epsilon_{ps}(c - c^*)$. The coupling term F_{ps} should be regarded as the first term in an expansion. A more precise study should take into account higher order terms, particularly in the surfactant concentration c .

For water-soluble polymers, hydrogen bonds play an important role because of the strong polarity of water molecules and more refined expressions for F_p and F_{ps} should be used. For example, the phase diagram of water-soluble polymers like poly(ethylene oxide) (PEO) exhibits closed loops of immiscibility and the definition of good solvent conditions is somewhat vague.³

We are not aware of many experiments performed on adsorption of polymers on a Langmuir monolayer, which will allow a direct comparison with our results.⁷ Interesting

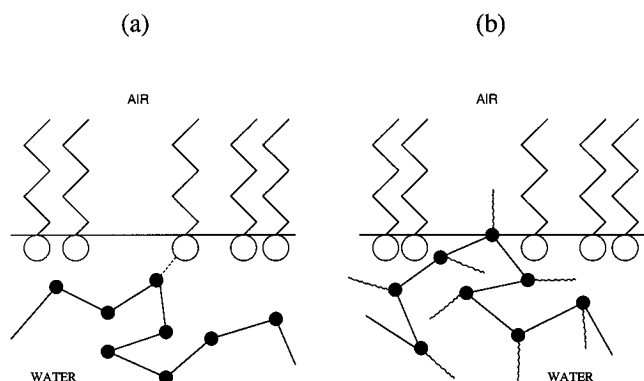


Figure 7. Two different kinds of interaction between the monomers and the interface. In (a), monomers interact with surfactant molecules either attractively (for instance, as a consequence of favorable van der Waals interactions) or repulsively (if, on the contrary, water is a good solvent for both molecules, and the surfactant heads act as a polymer brush). In (b), an associating polymer is shown; the hydrophobic subchains tend to dispose themselves in the air subphase and consequently attract the polymer chain close to the interface. (Adapted from ref 22.)

polymers that can be used experimentally to test our theory are hydrophobically modified water-soluble polymers (HM-WSP).^{6,8–11} These *associating* copolymers are attracted by the bare interface because of short hydrophobic side chains, attached covalently to the main chain. By adjusting the number and the length of the side chains, one can directly modify their surface affinity. In our model it corresponds to γ_0 , the parameter of interaction between the polymer and the bare surface.

Figure 7 shows two different kinds of interaction between the monomers and the interface. In (a), monomers interact with the interface through any kind of short-ranged interaction: either attractive or repulsive. In (b), the attraction of HM-WSP polymers towards the interface is illustrated: one of the aliphatic side chains of a HM-WSP polymer is in a low energy state in the air subphase. The monomers of the main chain covalently bound to this aliphatic group are consequently attracted in the region of the interface.

The HM-WSP polymers can be used to study systematically the dependence of the phase diagram on the special transition concentration c^* (as well as on the coupling parameter ϵ_{ps}), including the interesting situation where the special transition line intersects the phase diagram ($0 < c^* < 1$) because the polymer is repelled from the surfactant molecules ($\alpha_0 < 0$). The surfactant can be chosen as nonionic, with a polar head (hydrophilic) identical to the monomers, resulting in a repulsion between the “brush” (formed by the polar heads) and the polymer (water being a good solvent for both).^{22,29} The resulting coupling parameter ϵ_{ps} is negative and the triple point occurs for values of c^* close to zero and not close to unity as when $\epsilon_{ps} > 0$ (Figure 5). However, such polymers usually have a complicated behavior in the bulk and their self-assembly properties may be crucial. Another possible candidate for experiments may be a polymer with a “simpler” behavior in water, like PEO, having a surface affinity.³³ Probably here one needs to treat more explicitly the hydrogen bonds.

The parameters in the model can also be tuned by changing the surfactant characteristics. Pentadecanoic acid, for example, whose gaseous to liquid expanded transition has already been studied by several authors,^{34,35} can probably be an interesting surfactant to use.

In a previous work,²² several phase diagrams for the mixed polymer–surfactant system have been proposed from qualitative and general arguments. The proposed phase diagrams exhibit

the special transition line for the polymer ($c = c^*$) and the coexistence line for the surfactant molecules, but the interaction between these two lines was not treated in detail. Our results suggest that the position of the special transition line has a very strong effect on the position of the coexistence line. Reference 22 also predicted a Θ line separating a region where the polymer segregates from the surfactant from a region where the polymer and surfactant are mixed together. Our mean-field model does not address directly this prediction since we have only one minimum of the polymer surface value ϕ_s as a function of surfactant coverage c (see eq 2.9), and we assume that the polymer solution is homogeneous in the directions parallel to the interface as long as the surfactant monolayer is homogeneous.

From our study it seems that the Θ line of ref 22 and the coexistence line are the same: regions of different concentrations for the polymer correspond to regions of different concentrations for the surfactant. The polymer can be attracted to the interface and segregates from the surfactant only if it is attracted by the bare interface but repelled by the surfactant molecules. This situation is driven by energy terms which are first order in the polymer concentration (see eq 2.7) and is consequently different from the one predicted in ref 22. It will be interesting to understand in a detailed way this discrepancy, especially for $0 < c^* < 1$, where the coupling between the special transition and the surfactant phase diagram leads to the richest variety of phenomena.

5. Conclusions

We addressed in detail the adsorption of a semidilute polymer solution on a surfactant monolayer and the resulting phase diagrams. In our model, the most important degree of freedom is the local concentration c of surfactant at the interface. Since the monomers interact with regions of different concentrations with an energy proportional to $c - c^*$ (c^* is the concentration at the *special transition*), a rich variety of phenomena results from the coupling between the polymer solution and the surfactant monolayer. The polymer surface excess is enhanced and the phase diagrams of the surfactant monolayer are modified. The monomers induce an additional indirect attraction between the surfactant molecules depending on the concentration of surfactant on the interface. Consequently, the range of the homogeneous region in the phase diagram decreases. When the monomers interact more favorably with the surfactant molecules than with the bare interface, the critical concentration itself increases.

The value of the special transition coverage c^* , describing the interaction of the monomers with the surfactant molecules relative to their interaction with the bare water/air interface, has a major effect on the phase diagram of the surfactant monolayer. When the monomers are repelled by the surfactant molecules as well as by the bare interface (for instance, $\epsilon_{ps} > 0$ and $c^* > 1$), the phase diagram is not very different from the one of a simple surfactant monolayer without polymer in the water subphase. On the other hand, when the monomers are attracted by the surfactant molecules as well as by the bare interface (for instance, $\epsilon_{ps} > 0$ and $c^* < 0$), the increase of the two-phase region can be important. In the intermediary situation when the polymer is attracted to the interface or depleted ($0 < c^* < 1$), these two scenarios are in competition leading to a rich phase behavior and, in some cases, the phase diagram displays two critical points and one triple point (as in Figures 5 and 9k).

Finally, we mention two possible extensions of the present study. The first is to consider the situation of soluble surfactants and to take into account the complex surfactant–polymer

interactions in the bulk. Interesting experimental results have been obtained for such systems.¹¹ Moreover, our model can easily be adapted to mixed monolayers with two components. Such binary mixtures have been shown to exhibit immiscibility at room temperature, (e.g., for cholesterol and dimyristoylphosphatidylcholine (DMPC))^{36,37}). The understanding of the features of this phase transition may help to understand interactions of polymers with flexible membranes (lipid bilayer) and the phenomenon of *budding* of membranes.^{1,2,38,39}

Acknowledgment. We greatly benefited from discussions and correspondence with P.-G. de Gennes, H. Diamant, J. F. Joanny, B. Menes, and S. Safran. Partial support from the German–Israel Foundation (GIF) under Grant No. I-0197 and the US–Israel Binational Foundation (BSF) under Grant No. 94-00291 is gratefully acknowledged. One of us (X.C.) acknowledges support from the French Ministry of Foreign Affairs as well as from the ENS Lyon.

Appendix A: The Spinodal Equation

The general equation of the free energy of the system, as was derived in section 2, is

$$F = \nu^{-1}c(1-c) + c \log c + (1-c) \log(1-c) - \frac{\epsilon_p}{6}(\phi_s^3 + 3\phi_s - 4) \quad (\text{A.1})$$

If we do not assume any specific temperature dependence for ν , ϵ_p , ϵ_{ps} , and c^* , the global phase diagram has to be studied in the five-dimensional space of ν , ϵ_p , ϵ_{ps} , c^* , and c . The binodal and the spinodal surfaces are four-dimensional hypersurfaces in this five-dimensional space. We shall consider both positive and negative ν . It is worthwhile to investigate the spinodal surface because it can be done analytically, and it roughly describes the phase separation region, since the spinodal surface lies always within the coexistence region. The surface of instability (spinodal surface) also indicates the locations of possible critical points. For fixed values of ϵ_p , ϵ_{ps} and c^* , spinodal equation 3.1 describes cuts of the spinodal surface by the curve $\nu^{-1} = \nu^{-1}(c)$

$$2\nu^{-1} = \frac{1}{c(1-c)} - \frac{\epsilon_{ps}^2}{\epsilon_p} \frac{\phi_s^3}{\phi_s^2 + 1} \quad (\text{A.2})$$

It is interesting to look also at other cuts of the parameter space beside the (ν^{-1}, c) direction. An analytical expression can also be found in the (ϵ_p, c) direction (but not for the other interaction parameters).

Defining u as

$$u = \frac{c - c^*}{\epsilon_{ps}} \left(\frac{1}{c(1-c)} - 2\nu^{-1} \right) \quad (\text{A.3})$$

we note that $u = 0$ for both the special transition line and the spinodal line of the noncoupling case ($F(c) = F_s(c)$). From spinodal equation A.2 it follows that, if ϵ_p is a solution of the spinodal equation 3.1, ϵ_p^2 is the solution of a bi-quadratic equation:

$$4u^2\epsilon_p^4 - \lambda^2(1 + 4u - u^2)\epsilon_p^2 - \lambda^4u = 0 \quad (\text{A.4})$$

Alternatively, it can be shown that, if ϵ_p is a solution of (A.4), then, either ϵ_p or $-\epsilon_p$ is a solution of spinodal equation 3.1. As the polymer is supposed to be in good solvent conditions, we disregard negative solutions of the spinodal equation for ϵ_p . The

second order equation for ϵ_p^2 (eq A.4) may have either only one real solution or even no real solution at all, depending on its discriminant. Furthermore, only positive solutions should be taken into account, since $\epsilon_p^2 > 0$. All these considerations give several bounds to the possible values of u and λ . The roots of bi-quadratic equation A.4 are

$$\beta_{\pm} = \frac{\lambda^2}{8u^2} \left(1 + 4u - u^2 \pm (u+1)\sqrt{1+6u+u^2} \right) \quad (\text{A.5})$$

When β_+ is real and positive, only one solution of the spinodal equation exists: either $\epsilon_p = \sqrt{\beta_+}$ or $\epsilon_p = -\sqrt{\beta_+}$. We shall consider this solution only in the case when it is positive. The same can be said for β_- .

Defining $u_0 = -3 + \sqrt{8} \approx -0.1716$, we separate three cases for the roots of eq A.4 given by eq A.5:

1. For $u > 0$, β_+ is real and positive (while β_- is negative and, therefore, irrelevant). Hence, there is only one solution for ϵ_p .
2. For $u_0 \leq u \leq 0$, β_+ and β_- are both real and positive (for $u \rightarrow 0$, $\beta_- \rightarrow 0$). Hence, there are two solutions for ϵ_p .
3. For $u < u_0$, neither β_+ nor β_- is real and positive. Hence, there is no physical solution for ϵ_p .

Once ϵ_{ps} and c^* are fixed, ϵ_p is a function of ν and c . It is instructive to identify the domains in the (ν, c) plane where spinodal equation 3.1 has zero, one, or two real solutions. This requires locating the lines $u = 0$ and $u = u_0$. Depending on the values of ϵ_{ps} and c^* , two different situations are identified and shown in Figure 8. In particular, it can be seen in Figure 8b that, for $1/2 < c^* < 1$, there can be a range of values for ν^{-1} where cuts of the spinodal surface in the plane (ϵ_p, c) are disconnected (if ϵ_{ps} is below a certain critical value). For instance, in Figure 9j ($1/2 < c^* = 0.86 < 1$), a cut of the phase diagram at $\nu_0^{-1} < \nu^{-1} = 1.8 < \nu_1^{-1}$ is presented. The spinodal line is defined for two disconnected regions of concentration: one centered around $c = 0.6$ and one at higher concentrations.

Appendix B: The Global Phase Diagram

The phase diagram for the surfactant monolayer, including the surfaces of instability and coexistence, is presented in the three-dimensional parameter space of ν^{-1} , ϵ_p , and c through several cuts in two dimensions (ϵ_p and c), while fixing the other two parameters, ϵ_{ps} and c^* . We first discuss some general features of the phase diagram, starting with the simple case of no *effective* coupling between the polymer and the interface ($\epsilon_{ps} = 0$; $F(c) = F_s(c)$) as a reference point. The dependence of the phase diagram on the position of the special transition line is then studied, and the phase diagrams are presented for the cases $c^* < 0$, $c^* > 1$, and $0 < c^* < 1$.

When there is no *effective* coupling between the polymer solution and the surfactant monolayer, $\epsilon_{ps} = 0$ and the special transition line is not defined. The concentration of the polymer at the interface depends on the strength of the interaction between the monomers and the interface, $\alpha_0 = \gamma_0 = \lambda$. The phase separation in the monolayer was explained in section 2.1, and all its features are independent on the polymer parameter ϵ_p . In the plane (ν^{-1}, c) , the line $\nu^{-1} = 1/[2c(1-c)]$ delimits the unstable region (see Figure 8). From eq A.2 it appears that as soon as there is a nonzero effective coupling, the line of instability occurs for smaller values of ν^{-1} . This means that the coupling enlarges the region of instability of the homogeneous state. Consequently, the dark shaded region inside the line $\nu^{-1} = 1/[2c(1-c)]$ in Figure 8 is always a zone of instability, for any value of the parameters ϵ_p , ϵ_{ps} , and c^* . When ϵ_p is big, the polymer “stiffness” induces the polymers in

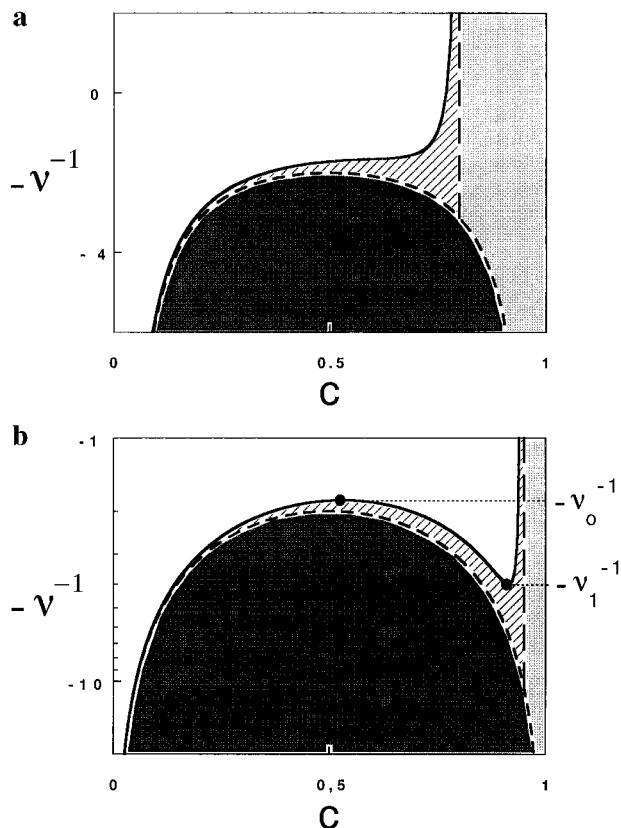


Figure 8. Regions of definition of the spinodal hypersurface in the plane $(-\nu^{-1}, c)$ for (a) $\epsilon_{ps} = 1$ and $c^* = 0.8$, (b) $\epsilon_{ps} = 1$ and $c^* = 0.95$. The full line is the $u = u_0$ line defined in Appendix A. The curved dashed line is the line of instability for the noncoupling case: $2\nu^{-1} = 1/[c(1-c)]$; the vertical dashed line is the line $c = c^*$. The region where only the solution β_+ is real and positive and generates a positive solution ϵ_p to the spinodal equation is lightly shaded, while the region where both solutions β_+ and β_- are real and positive and generate a positive solution ϵ_p is hashed. The dark shaded region is the zone where the surfactant monolayer is always unstable. The region above the full line ($u = u_0$) is a zone where neither β_+ nor β_- is real and positive. In (b), the $u = u_0$ line has two extrema at $\nu = \nu_0$ and $\nu = \nu_1$.

solution to be uniform, and the coupling acts as a chemical potential having a value $(1/2)\epsilon_{ps}$, as can be seen from eq 2.10 (after expanding ϕ_s to first order in powers of ϵ_p^{-1}). In this limit, the properties of the phase separation are the same as in the noncoupling case. Considering the cuts of the phase diagram in the direction (ϵ_p, c) for $\epsilon_{ps} = 0$, there are two different regions of the parameter space: (1) the region $\nu^{-1} < 2$, where there is no instability and no phase separation, and (2) the region $\nu^{-1} > 2$, where there is a phase separation.

Figure 9a shows the spinodal and the binodal lines for $\nu = 2.31$. Both lines are vertical because the properties of the phase transition are independent of ϵ_p , as was already explained above. In the limit $\nu^{-1} \rightarrow 2$, the phase diagram reduces to a line of critical points parallel to the ϵ_p axis at $c = 0.5$. The coupling results in a deformation of the line of critical points and enlarges the phase coexistence region. The cuts of the phase diagram in the direction (ϵ_p, c) for $\nu^{-1} < 2$ are topologically very different from the cuts obtained for $\nu^{-1} > 2$, because the latter necessarily contain the region of instability of the noncoupling situation (even for large values of ϵ_p), while, for the former, large values of ϵ_p necessarily correspond to domains of stability of the monolayer.

We first discuss the cases where the special transition line $c = c^*$ does not intersect the parameter space ($c^* < 0$ or $c^* > 1$). The phase diagrams are constructed by numerical solution of eqs 3.1 and 3.2.

B.1. The $c^* < 0$ Case. When both the surfactant and the interface attract the monomers, two situations can occur: if $\alpha_0 > \gamma_0 > 0$, then $\epsilon_{ps} > 0$ and $c^* \leq 0$. But if $\gamma_0 > \alpha_0 > 0$, $\epsilon_{ps} < 0$ and $c^* \geq 1$. However, as was explained at the beginning of section 2.4, these two situations can be mapped onto each other. Therefore, we concentrate here on the case $\epsilon_{ps} > 0$ and $c^* \leq 0$. The only relevant solution of the spinodal equation for ϵ_p is then $\epsilon_p = +\sqrt{\beta_+}$, defined outside of the region of instability of the noncoupling case. When ϵ_p is big, the polymer stiffness enforces the polymer solution to be uniform, $\phi_s \approx 1$, and the monomers exert a strong uniform attraction on the surfactant molecules.

For $\nu^{-1} < 2$, there is a phase separation, provided that ϵ_p is small enough. This is shown in Figure 9b, where it can be seen that the spinodal and the binodal lines join at a critical point. When ν^{-1} is changed, the basic topology of the binodal and spinodal lines remains unchanged. But, in the limit $\nu^{-1} \rightarrow 2^-$, close to the region where a phase separation occurs even without a coupling, the value of ϵ_p at the critical point increases. Moreover, the critical concentration tends to the value of the noncoupling case $c = 1/2$ (because ϵ_p at the critical point is large). If, on the other hand ν^{-1} decreases, the value of ϵ_p at the critical point decreases and the critical concentration c_c increases, $c_c \rightarrow 1$ when $\nu^{-1} \rightarrow -\infty$.

For $\nu^{-1} > 2$, the phase diagram is presented in Figure 9c. There is no critical point because the phase separation occurs for all values of ϵ_p . For $\epsilon_p \rightarrow 0$, the effects of the coupling between the monomers and the surfactant molecules are the strongest: the polymer is strongly attracted to the interface, particularly in the regions dense in surfactant. As a result, the surfactant molecules aggregate with a close-packing coverage $c = 1$.

B.2. The $c^* > 1$ Case. The opposite situation happens when both the surfactant and the bare interface repel the monomers. As explained above, it is enough to consider only $\epsilon_{ps} > 0$ and $c^* \geq 1$. In this situation, the function $\nu^{-1}(c)$ defined by the line $u = u_0$ in the plane (ν^{-1}, c) (see Appendix A) has a minimum $\nu_0^{-1} < 2$, which is a function of ϵ_{ps} and c^* . When $\nu^{-1} < \nu_0^{-1}$, then $u < u_0$. The spinodal equation has no solution and the homogeneous monolayer state is stable. For $\nu^{-1} > \nu_0^{-1}$, from a topological point of view, the spinodal surface is deformed for intermediate values of ϵ_p . Whereas for large values of ϵ_p the polymer remains stiff and the properties of the phase transition are those of the noncoupling case, for small values of ϵ_p the repulsion of the interface is dominant. The polymer is strongly depleted and the coupling has no effect.

The cuts of the phase diagram in the direction (ϵ_p, c) have the following features:

1. For $\nu_0^{-1} < \nu^{-1} < 2$ the phase diagram has a closed-loop immiscibility curve with an upper and a lower critical points as shown on Figure 9d. When $\nu^{-1} \rightarrow 2^-$, the upper critical point tends to ∞ and the lower one to 0, whereas when $\nu^{-1} \rightarrow \nu_0^{-1}$, the domain of instability becomes very small.

2. For $\nu^{-1} > 2$, there is a phase separation, whose characteristics differ from the one of the noncoupling case only for intermediate values of ϵ_p . An example of such a case is presented in Figure 9e.

The line of critical points has only, for intermediate values of ϵ_p , a small distortion with respect to the straight line of the noncoupling case. One consequence is that there is a maximal value for the critical concentration. When c^* is increased, the repulsion from the interface increases and the phase diagram resembles the noncoupling case, even at intermediate values of ϵ_p .

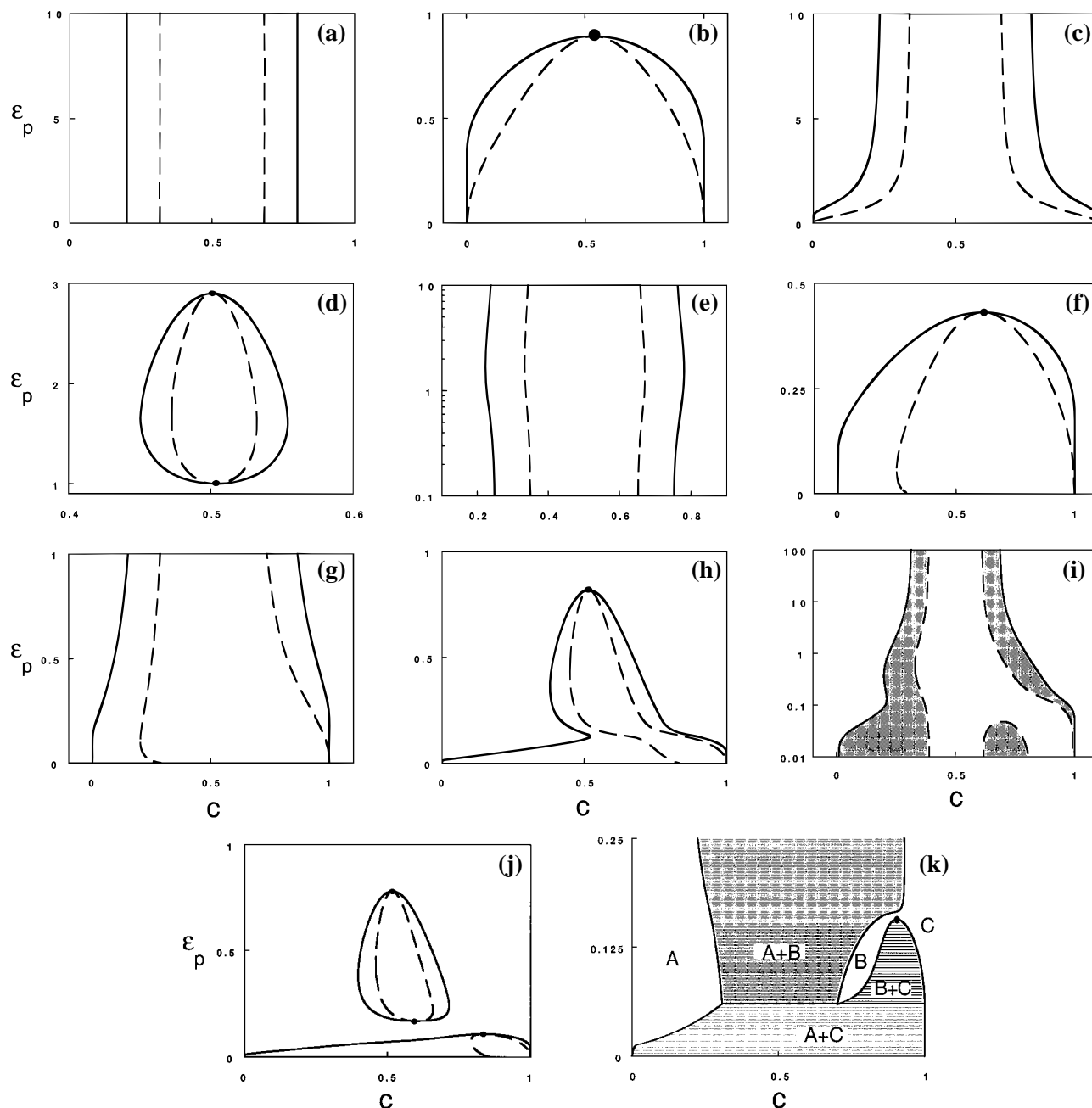


Figure 9. Cuts of the phase diagram in the (ϵ_p, c) plane. The full lines represent the binodal surface, while the dashed lines represent the spinodal surface. Critical points are shown by a dot. (a) $\nu^{-1} = 2.31$ and $\epsilon_{ps} = 0$; this plot shows the reference situation of the noncoupling surface. The next plots illustrate the text of Appendix B, in the three cases $c^* \leq 0$, $c^* \geq 1$, and $0 \leq c^* \leq 1$. In (b) to (j) $\epsilon_{ps} = 1$. (b) $\nu^{-1} = 1$ and $c^* = -1$; (c) $\nu^{-1} = 2.2$ and $c^* = -1$; (d) $\nu^{-1} = 1.95$ and $c^* = 2$. This plot shows a closed-loop phase diagram. (e) $\nu^{-1} = 2.2$ and $c^* = 2$. The ϵ_p scale in this plot is logarithmic for convenience. (f) $\nu^{-1} = 1$ and $c^* = 0.3$; (g) $\nu^{-1} = 2.2$ and $c^* = 0.3$; (h) $\nu^{-1} = 1.8$ and $c^* = 0.84$. This phase diagram displays a reentrant phase. (i) $\nu^{-1} = 2.1$ and $c^* = 0.84$. The ϵ_p scale in this plot is logarithmic for convenience, and the shaded region corresponds to the metastable states. (j) $\nu^{-1} = 1.8$ and $c^* = 0.86$. This plot shows a disconnected phase diagram. In (k) $\nu^{-1} = 2.1$, $\epsilon_{ps} = 2.1$, and $c^* = 0.95$. A first two-phase region A+B extends to infinite values for ϵ_p ; the second two-phase region ends at a critical point $c_c = 0.90$, $(\epsilon_p)_c = 0.16$; all three two-phase regions, A+B, A+C and B+C, join at a *triple point*— $\epsilon_p = 0.06$, $c_A = 0.30$, $c_B = 0.70$, and $c_C = 0.99$ —where all three phases (A, B, and C) coexist.

B.3. The $0 < c^* \leq 1$ Case. We turn now to the more complex case where the special transition line intersects the physical range of parameter space ($0 < c < 1$). The situation for $0 < c^* < 1/2$ is rather simple, the two typical phase diagrams are shown in Figure 9f (for $\epsilon_{ps} < 2$) and 9g (for $\epsilon_{ps} > 2$). They resemble the $c^* < 0$ case. However, for $1/2 < c^* < 1$, depending on the value of the coupling parameter ϵ_{ps} , the competition between the different terms in the free energy leads to a large variety of possible phase diagrams. An example of a phase diagram with a reentrant phase is presented in Figure 9h. In Figure 9i yet another type of phase diagram is presented

where a second metastable region resides inside the two-phase region. In some cases, as was suggested at the end of Appendix A, the phase diagram appears as if it is composed of two disconnected parts (those are cuts obtained for $\nu_0^{-1} < \nu^{-1} < 2$). An example is given in Figure 9j. Note that for $2 < \nu^{-1} < \nu_1^{-1}$ the spinodal surface is disconnected while the binodal surface is connected, since at very low values of ϵ_p a phase separation always occurs between very dense ($c \approx 1$) and very dilute ($c \approx 0$) regions (for $c^* < 1$), as is explained below. In the three dimensions $(\epsilon_s, \epsilon_p, c)$, the phase diagram is always connected: when ν^{-1} is increased the disconnected parts of the

phase diagram meet and this may result in the appearance of a triple point for a range of values for ϵ_s (an example is shown in Figure 9k). These triple points occur only for a small range of values for ϵ_p , typically, for $\epsilon_p \approx 0.1$.

Note that in all these phase diagrams (Figure 9f–k), the binodal line at low values of ϵ_p always ends at $c = 0$ and $c = 1$. It can be understood since for low values of ϵ_p , regions of surfactant concentrations $c < c^*$ (and outside of the region of instability of the noncoupling case) are not unstable because they repel the monomers, and the coupling consequently does not have any effect. The free energy is unchanged as compared to the noncoupling case. However, it is strongly modified for $c > c^*$, as has been explained in section 3.6 and is shown in Figure 4a. The common tangent construction results in a couple of stable coexistence points ($c \approx 0$, $c \approx 1$). Therefore, the regions of surfactant concentrations $c < c^*$ (and outside of the region of instability of the noncoupling case) are metastable.

Appendix C: The Critical Point

It is possible to obtain analytical results for the critical point, by solving simultaneously eqs 3.1 and 3.2 for the two unknowns: the critical concentration c_c and the critical temperature.

C.1. Bounds on the Critical Concentration. In general, no analytical expression for the critical concentration c_c exists but we derive an analytical expression for an upper bound. Equation 3.2 can be rewritten as a third order equation for ϕ_s^2 :

$$\phi_s^6 + 3\phi_s^4 + 3f(c)\phi_s^2 + f(c) = 0 \quad (\text{C.1})$$

where the coefficient $f(c)$ is defined as

$$f(c) = \frac{1 - 2c}{(1 - 2c) + c^2(1 - c)^2\epsilon_{ps}^3/\epsilon_p^2} \quad (\text{C.2})$$

We denote c_1 as the value of the surfactant concentration for which $f(c)$ diverges. A careful study of eq C.1 shows that $f(c) < 0$ and yields a nonanalytical solution for ϕ_s and consequently for c_c . It can also be shown that $1/2 < c_c < c_1$. From its definition, c_1 is the solution of a fourth order equation and has a (complicated) analytical expression as an odd increasing function of $\epsilon_{ps}^3/\epsilon_p^2$. For $\epsilon_{ps}^3/\epsilon_p^2 = 0$, $c_1 = 1/2$, and when $\epsilon_{ps}^3/\epsilon_p^2 \rightarrow \infty$, $c_1 \rightarrow 1.40$.

C.2. The Critical Point in the Strong-Coupling Limit. Hereafter we concentrate on the specific case of the strong-coupling limit, where ν^{-1} can be neglected in spinodal equation 3.1

$$\phi_s^2 + 1 = \epsilon_{ps}^2 \phi_s^3 \frac{c(1 - c)}{\epsilon_p} \quad (\text{C.3})$$

Taking the polymer order parameter ϵ_p and the special transition c^* as known parameters, the characteristics of the critical point can be determined by solving a system of three equations (spinodal equation C.3, eq 3.2, and the definition of ϕ_s (eq 2.9)) with three unknowns: the concentration of surfactant c , the temperature appearing through ϵ_{ps} , and ϕ_s (which has been added for mathematical convenience). First, bounds on the critical concentration are obtained, depending only on the special transition concentration. then, a method of determination of the critical concentration is discussed. Using eq C.3, eq 3.2 can be rewritten as a second order equation for ϕ_s^2 .

As there is at least one real and positive solution to this equation, a bound on the value of the critical concentration,

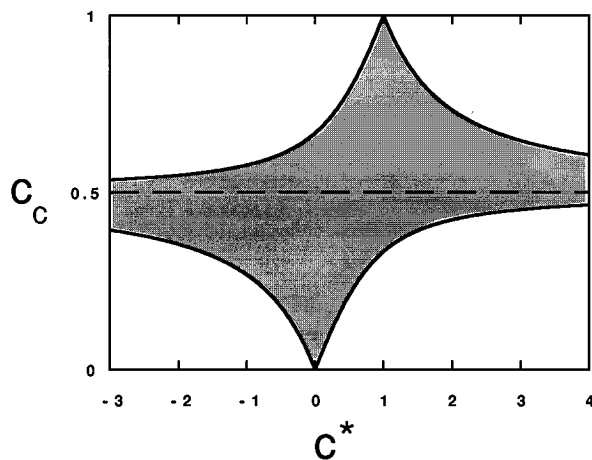


Figure 10. Range of critical concentration c_c as a function only of the special transition concentration c^* in the strong-coupling limit; shown inside the shaded region.

depending only on the special transition concentration c^* is obtained (Figure 10).

For $c^* \leq 0$:

$$1 - c^* - \sqrt{c^{*2} - c^* + 1} \leq c_c \leq \left(\frac{1}{3}\right) \left[(c^* + 1) + \sqrt{c^{*2} - c^* + 1} \right]$$

For $0 \leq c^* \leq 1$:

$$\left(\frac{1}{3}\right) \left[(c^* + 1) - \sqrt{c^{*2} - c^* + 1} \right] \leq c_c \leq \left(\frac{1}{3}\right) \left[(c^* + 1) + \sqrt{c^{*2} - c^* + 1} \right]$$

For $c^* > 1$:

$$\left(\frac{1}{3}\right) \left[(c^* + 1) - \sqrt{c^{*2} - c^* + 1} \right] \leq c_c \leq \frac{1 - c^* + \sqrt{c^{*2} - c^* + 1}}{3}$$

For $c^* = 0$, this bound is $0 < c_c < 2/3$. Therefore, if the effective coupling parameter ϵ_{ps} is positive, we know that the critical concentration obeys $1/2 < c_c < 2/3$.

The second order equation for ϕ_s^2 can be rewritten as a second order equation for the critical concentration c_c , depending on the special transition c^* and on the concentration of monomers at the interface ϕ_s :

$$[4 - 3(\phi_s^2 + 1)^2]c_c^2 - 2[2 - (1 + c^*)(\phi_s^2 + 1)]c_c - c^*(\phi_s^2 + 1)^2 = 0 \quad (\text{C.4})$$

The study of this equation shows the following:

For $c^* = 0$ or $c^* = 1$, it reduces to a first order equation.

For $c^* < 0$,

$$c_c = c_- \equiv \left[2 - (1 + c^*)(\phi_s^2 + 1)^2 - \sqrt{(\phi_s^2 + 1)^4(c^{*2} - c^* + 1) - 4(\phi_s^2 + 1)^2 + 4} \right] / \left[4 - 3(\phi_s^2 + 1)^2 \right]$$

For $c^* > 1$,

$$c_c = c_+ \equiv \left[2 - (1 + c^*)(\phi_s^2 + 1)^2 + \sqrt{(\phi_s^2 + 1)^4 (c^{*2} - c^* + 1) - 4(\phi_s^2 + 1)^2 + 4} \right] \left[4 - 3(\phi_s^2 + 1)^2 \right]$$

For $0 < c^* < 1$, the situation is more complicated. It can be shown, in particular, that there is a minimum for the concentration of the monomers at the interface at the critical point. This minimal value always corresponds to a situation of depletion for the polymer solution. It can also be shown that in some situations, when $\epsilon_{ps} > 0$ and $1/2 < c^* < 1$ or symmetrically when $\epsilon_{ps} < 0$ and $0 < c^* < 1/2$, the solutions c_- and c_+ may be relevant: this accounts for the possibility of two critical points. The definition of ϕ_s (eq 2.9) can be rewritten as

$$\phi_s^2 - 1 = \frac{\epsilon_{ps}}{\epsilon_p} \phi_s (c - c^*) \quad (\text{C.5})$$

ϵ_{ps} can be eliminated from spinodal equation C.3 by using its expression obtained from eq C.5. On the other hand, the concentration can be substituted by using its expression $c_-(\phi_s, c^*)$ or $c_+(\phi_s, c^*)$. One is left with a high order polynomial equation for ϕ_s depending only on the special transition concentration c^* and the polymer interaction parameter ϵ_p . Once this equation is numerically solved, the other characteristics of the critical point (concentration, temperature) are easily obtained as simple function of ϕ_s . In particular, once the critical concentration is known, the critical ϵ_{ps} , hence the critical temperature, is obtained from eq C.5.

References and Notes

- (1) Sackmann, E. *FEBS Lett.* **1994**, *346*, 3.
- (2) Bloom, M.; Evans, E.; Mouritsen, O. G. *Q. Rev. Biophys.* **1991**, *24*, 293.
- (3) Napper, D. H. *Polymeric Stabilization of Colloidal Dispersions*; Academic: London, 1983.
- (4) Goddard, E. D.; Ananthapadmanabhan, K. P. *Polymer Surfactant Interactions*; CRC: Boca Raton, FL, 1992.
- (5) Cabane, B.; Duplessix, R. *Colloids Surf.* **1985**, *13*, 19. Cabane, B.; Duplessix, R. *J. Phys. (Paris)* **1987**, *48*, 651.
- (6) Magny, B.; Iliopoulos, I.; Zana, R.; Audebert, R. *Langmuir* **1994**, *10*, 3180. Magny, B.; Iliopoulos, I.; Audebert, R.; Piculell, L.; Lindman, B. *Prog. Colloid Polym. Sci.* **1992**, *89*, 118.
- (7) Levy, M. Y.; Benita, S.; Baszkin, A. *Colloids Surf.* **1991**, *59*, 225.

- (8) Wang, T. K.; Iliopoulos, I.; Audebert, R. *Polym. Bull.* **1988**, *20*, 577.
- (9) Sarrazin-Cartalas, A.; Iliopoulos, I.; Audebert, R.; Olsson, U. *Langmuir* **1994**, *10*, 1421. Loyer, K.; Iliopoulos, I.; Audebert, R.; Olsson, U. *Langmuir* **1995**, *11*, 1053.
- (10) Nikas, Y. J.; Blankschtein, D. *Langmuir* **1994**, *10*, 3512.
- (11) Chari, K.; Hossain, T. Z. *J. Phys. Chem.* **1991**, *95*, 3302.
- (12) Gaines, G. L. *Insoluble Monolayers at Liquid-Gas Interfaces*; Interscience: New York, 1966.
- (13) Ulman, A. *An Introduction to Ultrathin Organic Films from Langmuir-Blodgett to Self-Assembly*; Academic: London, 1991.
- (14) Jacquemain, D.; Grayer Wolf, S.; Leveiller, F.; Deutsch, M.; Kjaer, K.; Als-Nielsen, J.; Lahav, M.; Leiserowitz, L. *Angew. Chem., Int. Ed. Engl.* **1992**, *31*, 130.
- (15) Fleer, G. J.; Cohen Stuart, M. A.; Scheutjens, J. M. H. M.; Cosgrove, T.; Vincent, B. *Polymers at Interfaces*; Chapman & Hall: London, 1993.
- (16) Richmond, P.; Lal, M. *Chem. Phys. Lett.* **1974**, *24*, 594. Jones, I. S.; Richmond, P. *J. Chem. Soc., Faraday Trans.* **1977**, *73*, 1062.
- (17) Joanny, J. F.; Leibler, L.; de Gennes, P. G. *J. Polym. Sci., Polym. Phys. Ed.* **1979**, *17*, 1073.
- (18) De Gennes, P. G. *Macromolecules* **1981**, *14*, 1637.
- (19) De Gennes, P. G. *Scaling Concepts in Polymer Physics*; Cornell University: Ithaca, NY, 1979.
- (20) Brooks, J. T.; Marques, C. M.; Cates, M. E. *Europhys. Lett.* **1991**, *14*, 713. Brooks, J. T.; Marques, C. M.; Cates, M. E. *J. Phys. II Fr.* **1991**, *1*, 673.
- (21) Hone, D.; Ji, H.; Pincus, P. A. *Macromolecules* **1987**, *20*, 2543.
- (22) Hone, D.; Ji, H. *Macromolecules* **1988**, *21*, 2600.
- (23) De Gennes, P. G. *J. Phys. Chem.* **1990**, *94*, 8407.
- (24) Odijk, T. *Macromolecules* **1990**, *23*, 1875.
- (25) Andelman, D.; Joanny, J. F. *J. Phys. II Fr.* **1993**, *3*, 121. Andelman, D.; Joanny, J. F. *Macromolecules* **1991**, *24*, 6040.
- (26) Châtelier, X.; Andelman, D. *Europhys. Lett.* **1995**, *32*, 567.
- (27) Bibo, A. M.; Knobler, C. M.; Peterson, I. R. *J. Phys. Chem.* **1991**, *95*, 5591.
- (28) Kaganer, V. M.; Loginov, E. B. *Phys. Rev. Lett.* **1993**, *71*, 2599.
- (29) Andelman, D.; Brochard, F.; Knobler, C.; Rondelez, F. In *Micelles, Membranes, Microemulsions and Monolayers*; Gelbart, W. M., Ben-Shaul, A., Roux, D., Eds.; Springer-Verlag: New York, 1994; Chapter 12.
- (30) Safran, S. *Statistical Thermodynamics of Surfaces, Interfaces and Membranes*; Addison-Wesley: Reading, MA, 1994; Chapter 1.
- (31) Edwards, S. F. *Proc. Phys. Soc.* **1965**, *85*, 613. Edwards, S. F. *Proc. Phys. Soc.* **1966**, *88*, 265.
- (32) We are indebted to S. Safran for this remark.
- (33) A more precise criterion for the validity of eq 3.3 is that $\nu\epsilon_{ps} \ll \epsilon_p/(|c - c^*|)$ and $\nu\epsilon_{ps} \ll \epsilon_p^{1/2}$. For a semidilute polymer solution, ϵ_p is in general very small with respect to unity (as was mentioned in section 2), and the low-coupling limit may hold only for very small values of $\nu\epsilon_{ps}$.
- (34) Bailey, F. E.; Callard, R. W. *J. Appl. Polym. Sci.* **1959**, *1*, 56.
- (35) Kim, M. W.; Cannell, D. S. *Phys. Rev. A* **1976**, *13*, 411.
- (36) Pallas, N. R.; Pethica, B. A. *J. Chem. Soc., Faraday Trans. 1* **1976**, *83*, 585.
- (37) Subramaniam, S.; McConnell, H. M. *J. Phys. Chem.* **1987**, *91*, 1715.
- (38) Seul, M.; Sammon, M. J. *Phys. Rev. Lett.* **1990**, *64*, 1903.
- (39) Sackmann, E. *Can. J. Phys.* **1990**, *68*, 1000.
- (40) Andelman, D.; Kawakatsu, T.; Kawasaki, K. *Europhys. Lett.* **1992**, *19*, 57.
- (41) As an indication for the variations of c_1 as a function of $\epsilon_{ps}^3/\epsilon_p^2$, $c_1(1) \approx 0.531$, $c_1(10) \approx 0.711$, $c_1(100) \approx 0.901$.

JP953680E